Stacking of Bacteriochlorophyll *c* Macrocycles in Chlorosome from *Chlorobium limicola* As Revealed by Intermolecular ^{13}C Magnetic-Dipole Correlation, X-Ray Diffraction, and Quadrupole Coupling in ^{25}Mg NMR[†]

Yoshinori Kakitani,[‡] Yasushi Koyama,*[,‡] Yuichi Shimoikeda,[§] Toshihito Nakai,[§] Hiroaki Utsumi,[§] Tadashi Shimizu,[||] and Hiroyoshi Nagae[⊥]

Faculty of Science and Technology, Kwansei Gakuin University, Gakuen, Sanda 669-1337, Japan, Analytical Instrument Division, JEOL Ltd., Musashino, Akishima, Tokyo 196-8558, Japan, National Institute for Materials Science, Sakura, Tsukuba, Ibaraki 305-0003, Japan, and Kobe City University of Foreign Studies, Gakuen-Higashimachi, Nishi-ku, Kobe 651-2187, Japan

Received August 31, 2008; Revised Manuscript Received November 14, 2008

ABSTRACT: The stacking of the bacteriochlorophyll (BChl) *c* macrocycles and the role of water in forming an aggregate sheet, in chlorosome, were examined by means of ^{13}C NMR spectroscopy, the measurement of the X-ray diffraction pattern, and ^{25}Mg NMR spectroscopy. (1) The stacking of the macrocycles, i.e., weakly overlapped dimers forming displaced layers, was selected out of six different kinds of stacking so far identified in the aggregates of isomeric BChl *c* in solution and in the solid aggregate of an isomeric mixture of BChl *c* extracted from *Chlorobium limicola*. The selection was based on the comparison of the intermolecular $^{13}C\cdots{}^{13}C$ magnetic-dipole correlations with the nearest-neighbor carbon-to-carbon close contacts simulated for the above six different stackings. It has turned out that the stacking of the macrocycles in chlorosome is basically the same as that in the *in vitro* solid aggregate. (2) The crucial role of water in stabilizing the aggregate structure in chlorosome was shown by tracing the dehydration processes and by comparison with the solid aggregate using the X-ray diffraction pattern. Possible binding sites of water molecules were located, by structural simulation, based on the particular stacking structure. (3) The dimer-based stacking of the macrocycles was evidenced by ^{25}Mg NMR spectroscopy, which exhibited a pair of signals showing different quadrupole coupling, due to the presence or absence of a water molecule in the axial position.

Green sulfur and non-sulfur bacteria have a unique antenna complex called "chlorosome", which mainly consists of a self-assembly of bacteriochlorophyll (BChl)[1] *c* and plays the important functions of light-harvesting and photoprotection (see refs *1*−*4*for reviews). It has been generally accepted that "the rod elements" forming cylindrical aggregates of BChl *c* were enveloped in a lipid monolayer in chlorosome. Historically, this picture of chlorosome was developed as follows: Chlorosome was first identified by electron microscopy of thin sections of the cells (*5*), and a more detailed structural analysis of negatively stained freeze-fractured samples was performed (*6*). The "rod" structures extending in parallel along the long axis of chlorosome were demonstrated in *Chlorobium limicola* (*7*). "A rod structure" coming out from the chlorosome envelope that was punctured by osmotic shock was photographed, and a more detailed model was built for the inside structure of chlorosome (*8*). However, the correlation between the morphological rod structure and the cylindrical aggregate of the BChl *c* molecules is still an open question.

Recently, the above picture of chlorosome was challenged, and a model of undulating lamella was proposed, instead (*9*). Importantly, electron micrographs and low-angle X-ray diffraction exhibited a key diffraction at ∼20 Å in chlorosome that were embedded in vitreous ice. However, the correlation between the morphological lamellar structure and the aggregate structure of BChl *c* has not been determined yet. Most recently, the long-range organization of BChl *c* aggregate in chlorosome from *Chlorobium tepidum* was investigated by cryoelectron microscopy (*10*). Interestingly, end-on views revealed that the chlorosome was composed of various multilayer tubes with some locally undulating nontubular lamella in between. A schematic model for the long-range organization of the BChl *c* layers that has been presented strongly suggested that "a self-assembly of BChl *c* forming a sheet-like structure" could be actually the basic structure of aggregate in chlorosome (*11*).

[†] This work has been supported by a grant "Open Research Center Project" (Y. Koyama) from the Ministry of Education, Culture, Sports, Science, and Technology (MEXT), Japan. Y. Kakitani has been supported by Grant-in-Aid for Scientific Research (C), 19579005, from MEXT, Japan.

* To whom correspondence should be addressed. Tel/Fax: +81-79-565-8408. E-mail: ykoyama@kwansei.ac.jp.

[‡] Kwansei Gakuin University.

[§] JEOL Ltd.

[||] National Institute for Materials Science.

[⊥] Kobe City University of Foreign Studies.

[1] Abbreviations: BChl, bacteriochlorophyll; *Chl.*, *Chlorobium*; CP, cross polarization; DARR, dipolar-assisted rotational resonance; MAS, magic angle spinning; NMR, nuclear magnetic resonance; NOE, nuclear Overhauser effect; *R*[E,E], (3^1R)-8-ethyl-12-ethyl bacteriochlorophyll c_F; RFDR, radio frequency-driven dipolar recoupling; *R*[P,E], (3^1R)-8-propyl-12-ethyl bacteriochlorophyll c_F; *S*[I,E], (3^1S)-8-isobutyl-12-ethyl bacteriochlorophyll c_F.

10.1021/bi801651w CCC: $40.75
Published on Web 12/12/2008

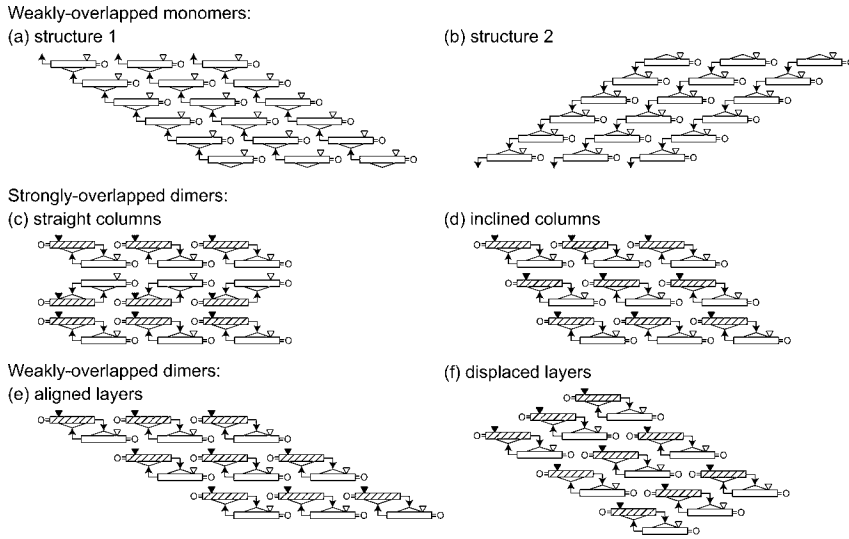

FIGURE 1: Schematic presentation for the various stackings of macrocycles we have identified in the previous investigations (see text). They can be classified into three different categories: "weakly overlapped monomers" forming (a) structure 1 and (b) structure 2, "strongly overlapped dimers" forming (c) straight and (d) inclined columns, and "weakly overlapped dimers" forming (e) aligned and (f) displaced layers. Each part of the BChl *c* molecule (see Scheme 1 for the chemical structure) is shown by the use of symbols: rectangle (the macrocycle), bent arrow (the hydroxyethyl group coordinating to the Mg atom), ═O (the keto-carbonyl group), and small triangle (the root of the farnesyl side chain). When viewed from the direction shown by an arrow in Scheme 1, those parts at the front are left open, whereas those parts at the back are shadowed or painted.

Scheme 1

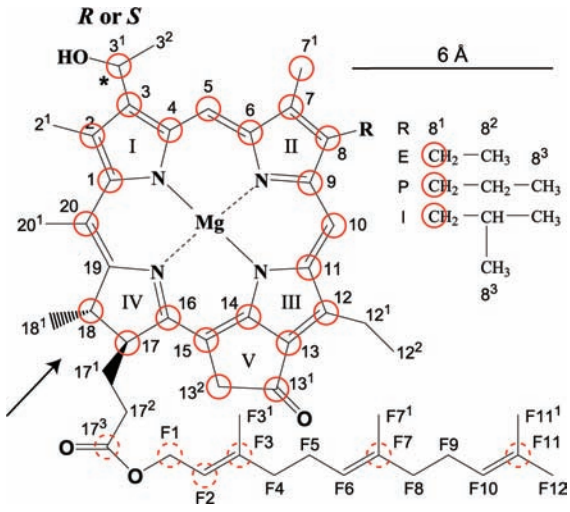

Now, we focus our attention on the short-range organization of the BChl *c* molecules to form an aggregate layer; Figure 1 presents six different stackings of macrocycles that we have identified so far by NMR spectroscopy. With respect to the long axis of a stacked column of macrocycles, the farnesyl side chains extend on one side in the monomer-based stacking of macrocycles, whereas they extend on both sides in the dimer-based stacking (see Scheme 1 for the chemical structure of BChl *c*). In both cases, the side chains taking various conformations prevent regular assembly of the columns to form a three-dimensional crystal structure; therefore, the assembly of the BChl *c* molecules is considered to be two-dimensional in nature.

To determine the assembly of BChl *c* molecules, ^{13}C cross-polarization/magic-angle-spinning (CP/MAS) nuclear magnetic resonance (NMR) spectroscopy played a most important role, and both the dimer-based stacking and the monomer-based stacking have been proposed based on the observed aggregation shifts and the simulated ring-current effects. Nozawa et al. (*12*) measured the ^{13}C CP/MAS NMR spectra of the intact chlorosome and the *in vitro* aggregate of extracted BChl *c* and concluded that the assemblies of the BChl *c* molecules were basically the same between them. They proposed a dimer-based stacking called "a direct ring overlap model" (*13*).

Holzwarth and Schaffner (*14*) examined the aggregate structure of methyl (3^1R)-bacteriochlorophyllide *d* by molecular modeling and proposed a monomeric stacking, instead. Balaban et al. (*15*) measured the 2D radiofrequency-driven dipolar-recoupling (RFDR) spectra and concluded that the 2D response of BChl *c* in the intact chlorosome is virtually indistinguishable from that of the *in vitro* aggregate. They also proposed a monomer-based stacking based on the high-field shifts of the $C2^1$, C3, $C3^2$, C5, $C12^1$, C13, and $C13^1$ resonances (see Scheme 1 for the typification of carbon atoms). van Rossum et al. (*16*) applied high-field heteronuclear 2D and 3D MAS NMR dipolar correlation spectroscopies to ^{13}C-enriched chlorosome to determine the ^1H chemical shifts; based on the high-field shifts around the peripheral part not only around ring I but also around rings III/V, they concluded a monomer-based stacking.

However, Wang et al. (*17*, *18*) concluded that the high-field shifts may *not* be due to the ring-current effects *but* due to the hydrogen bonding based on the detailed analysis of the relevant signals in the piggyback dimer of (3^1R)-8-ethyl-12-ethyl bacteriochlorophyll c_F (*R*[E,E]) in CCl_4 solution, supporting the dimer-based stacking.

Since the determination of the assembly of the BChl *c* molecules by the use of the aggregation shifts (ring-current effects) of the ^{13}C and ^1H signals turned out to be *contradictory*, we have decided to take a completely different approach, i.e., the determination of the stacking of macrocycles by comparison of the observed *intermolecular* $^{13}C\cdots{}^{13}C$ magnetic-dipole correlations with the simulated nearest-neighbor carbon-to-carbon close contacts based on various stackings that have been identified by ^1H and ^{13}C

NMR spectroscopy of *in vitro* aggregates. The isotope dilution method is the most reliable method to extract the intermolecular $^{13}C\cdots{}^{13}C$ magnetic-dipole correlation peaks out of a mixture of intramolecular and intermolecular correlation peaks in 2D magnetic-dipole correlation spectra; upon dilution of [^{13}C]BChl *c* from 100% to 50%, the *intramolecular* correlation peaks should decrease in intensity into $^1/_2$, whereas the *intermolecular* correlation peaks should decrease in intensity into $^1/_4$.

In a previous investigation, we have actually determined, by the use of this method, the assembly of BChl *c* in the *in vitro* solid aggregate of an isomeric mixture extracted from *Chl. limicola* (hereafter, we will call this sample simply "solid aggregate") (*19*). We found a unique stacking of macrocycles, as shown in Figure 1f, which we call "weakly overlapped dimers forming displaced layers". It consisted of (i) the dimer-based stacking, (ii) the pseudo-monomer-based stacking of structure 1 type, and (iii) the pseudo-monomer-based stacking of structure 2 type (see Figure 7 of ref *19*).

To apply this method to chlorosome, it was necessary to develop a technique to reassemble chlorosome, because the BChl *c* aggregates are *enveloped* in the lipid monolayer. We extracted two different pigment components from the cells that were grown in the ^{13}C and ^{12}C media and mixed them in a 1:1 ratio to assemble the chlorosome containing 50% [^{13}C]BChl *c*. The reassembled chlorosome was characterized to have similar but longer morphological structure, almost the same pigment assembly in the aggregate, and basically the same excited-state dynamics (*20*).

In the present investigation, we first applied a ^{13}C CP/MAS NMR technique called dipolar-assisted rotational resonance (DARR) to the reassembled chlorosome containing [^{13}C]BChl *c* and [^{12}C]BChl *c* in a 1:1 ratio to extract the *intermolecular* $^{13}C\cdots{}^{13}C$ magnetic-dipole correlations. Then, we compared the resultant magnetic-dipole correlations to the carbon-to-carbon close contacts simulated for a set of stackings of macrocycles so far identified. Second, we compared the X-ray diffraction pattern between chlorosome and solid aggregate to find difference in stacking of macrocycles, if any, and the structural role of water molecules. Finally, we applied recently developed ^{25}Mg NMR spectroscopy to chlorosome and solid aggregate to probe the electric-field gradient on the central Mg atom of macrocycle.

We have addressed the following four specific questions: (1) Does the aggregate structure in chlorosome consist of the monomer-based stacking or the dimer-based stacking? (2) What is the relation in the stacking of macrocycles between chlorosome and solid aggregate? (3) What is the specific role of water molecules in the aggregate structure in chlorosome? (4) What is the relevance of the overall aggregate structure in chlorosome to its physiological functions?

MATERIALS AND METHODS

Sample Preparations. The cells of *Chl. limicola* f. sp. *thiosulfatophilum*, of natural-abundance and ^{13}C-enriched isotopic composition, were grown anaerobically at 27 °C in dim light in the medium of Wahlund et al. (*21*), the details of which were described previously (*19*). Two kinds of reassembled chlorosome, i.e., one consisting of ^{13}C-enriched components only ("100% [^{13}C]BChl *c*") and the other consisting of a 1:1 mixture of the ^{13}C-enriched component and the component with the natural-abundance isotopic composition ("50% [^{13}C]BChl *c*"), were prepared by the use of the same method as described previously (*20*).

NMR Measurements. (A) ^{13}C NMR. All of the spectra were recorded on a JEOL ECA600 NMR spectrometer with a magnetic field of 14.096 T. A double resonance MAS probe equipped with a 4.0 mm o.d. rotor was used, which was tuned to ^{1}H and ^{13}C frequency at 600.17 and 150.9 MHz, respectively. The DARR technique (*22*) was used to obtain a set of spectra to determine the ^{13}C magnetic-dipole correlations. The spinning frequency of MAS was 10 kHz, the contact time was 2.0 ms, the mixing times were 50, 100, and 200 ms, and the data accumulation time was 17 h. The temperature of each sample was estimated to be around 30 °C. Each sample suspension was carefully sealed in the rotor to minimize the loss of water during MAS.

(B) ^{25}Mg NMR. Measurements of unlabeled chlorosome and solid aggregate were conducted on a JEOL ECA930 spectrometer under a magnetic field of 21.830 T where the ^{25}Mg resonance frequency was 56.897 MHz. A single-resonance MAS probe equipped with a 4.0 mm o.d. rotor was used, and the spinning frequency of MAS was 13 kHz. The signals were accumulated for 80 h in chlorosome and for 10 h in solid aggregate by using a single-pulse sequence with careful attention for the loss of water.

Model Building. Models of the aggregate of BChl *c* molecules were built by arranging a repeating unit, i.e., a monomer or a piggyback dimer, by the use of basically the same protocol described in ref *19*.

RESULTS AND DISCUSSION

Stacking of Macrocycles As Determined by Intermolecular $^{13}C\cdots{}^{13}C$ Magnetic-Dipole Correlations. (A) Stackings of Macrocycles So Far Identified. Figure 1 schematically presents various types of stacking of macrocycles we have identified in the previous investigations. The stackings include the monomer-based stacking and the dimer-based stacking, and they can be classified into three different categories: "weakly overlapped monomers" forming (a) structure 1 and (b) structure 2, "strongly overlapped dimers" forming (c) straight and (d) inclined columns, and "weakly overlapped dimers" forming (e) aligned and (f) displaced layers. Stackings (a)−(e) have been identified by high-resolution NMR spectroscopy of the lower aggregates of isolated BChl *c* isomers in solution (*23*−*27*), and stacking (f) by ^{13}C CP/MAS dipolar correlation spectroscopy of a solid aggregate of an isomeric mixture of BChl *c* ("solid aggregate") (*19*), the details of which will be described below.

Weakly overlapped monomers of BChl *c* forming staircase-like inclined columns, which extend to the opposite directions ((a) structure 1 and (b) structure 2), were found by high-resolution NMR spectroscopy of (3^1*S*)-8-isobutyl-12-ethyl bacteriochlorophyll c_F (*S*[I,E]) in a 1:3 mixture of methylene chloride and carbon tetrachloride by the use of the ^{1}H and ^{13}C aggregation shifts and the ^{1}H−^{1}H intermolecular nuclear Overhauser effect (NOE) correlations (*23, 24*). (c) Strongly overlapped dimers forming straight columns were identified by high-resolution NMR spectroscopy of *R*[E,E] in chloroform by the use of the ^{1}H and ^{13}C aggregation shifts and the

$^{1}H-^{1}H$ intermolecular NOE correlations (*25*). (d) Strongly overlapped dimers forming inclined columns were also identified in the same type of suspension by the use of the ^{1}H and ^{13}C aggregation shifts (*25, 26*). (e) Weakly overlapped dimers forming a staircase-like inclined column with aligned layers were identified by high-resolution NMR spectroscopy of (3^{1}*R*)-8-propyl-12-ethyl bacteriochlorophyll c_F (*R*[P,E]) in a mixture of methylene chloride and cyclohexane (1:14) by the use of the ^{1}H and ^{13}C aggregation shifts (*27*). (f) Weakly overlapped dimers forming a staircase-like inclined column with displaced layers were found by ^{13}C CP/MAS NMR spectroscopy of solid aggregate consisting of an isomeric mixture of BChl *c* extracted from *Chl. limicola* by the use of intermolecular $^{13}C\cdots^{13}C$ magnetic-dipole correlations extracted from the proton-driven spin-diffusion spectra (*19*).

(B) Extraction of Intermolecular Correlation Peaks. Figure S1 (in Supporting Information) shows the DARR spectrum of reassembled chlorosome (100% [^{13}C]BChl *c*; mixing time 100 ms); the assignment of the ^{13}C signals concerning the macrocycle and farnesyl side chain, which was determined by the use of an RFDR spectrum, is also indicated. The peak trains along the inclined lines are due to the side bands of MAS.

Figure 2 shows a set of DARR spectra that were recorded with mixing times of 50, 100, and 200 ms. Each pair of symmetrized spectra, in the form of triangles, consists of one for 100% [^{13}C]BChl *c* (top left) and the other for 50% [^{13}C]BChl *c* (bottom right). The *intermolecular* $^{13}C\cdots^{13}C$ dipolar correlation peaks, whose intensity decreases to $\sim^{1}/_{4}$ on going from 100% to 50%, are indicated by red solid circles for the macrocycle and by red broken circles for the farnesyl side chain. Table 1 lists these intermolecular $^{13}C\cdots^{13}C$ correlation peaks for the different mixing times thus extracted from the sets of DARR spectra. The numbers of observed correlation peaks at 50, 100, and 200 ms were 12, 15, and 15, respectively. Those carbon atoms exhibiting the intermolecular correlation peaks are indicated in Scheme 1 in red solid and broken circles for the macrocycle and farnesyl side chain, respectively. All of the observed carbon atoms are equally distributed around the macrocycle, a fact which supports reliable structural assessment.

(C) Selection of the Most Plausible Stacking of Macrocycles. Figure 3 compares, in the atomic number presentation, the observed intermolecular $^{13}C\cdots^{13}C$ magnetic-dipole correlations and the simulated nearest-neighbor carbon-to-carbon close contacts based on the six different stackings of macrocycles (see Figure 1). Table 2 summarizes the scores of agreement (in %) that are defined as the number of correctly predicted correlation peaks divided by the total number of the observed correlation peaks. The most plausible stacking has been selected as described below.

Weakly overlapped monomers forming either (a) structure 1 or (b) structure 2 stacking do not explain the observed correlation peaks in the diagonal region at all and explain those in the off-diagonal region only partially. The averaged scores of agreement are as low as 42% and 45% for (a) structure 1 and (b) structure 2, respectively.

(c) Strongly overlapped dimers forming straight columns explain the observed correlation peaks much better. As shown in Figure 1, this model contains the stacked pairs of macrocycles in parallel and in the same direction and, therefore, predicts such a large number of close contacts in the diagonal region; as a result, it gives rise to such a high averaged score of agreement, 74%. However, this stacking

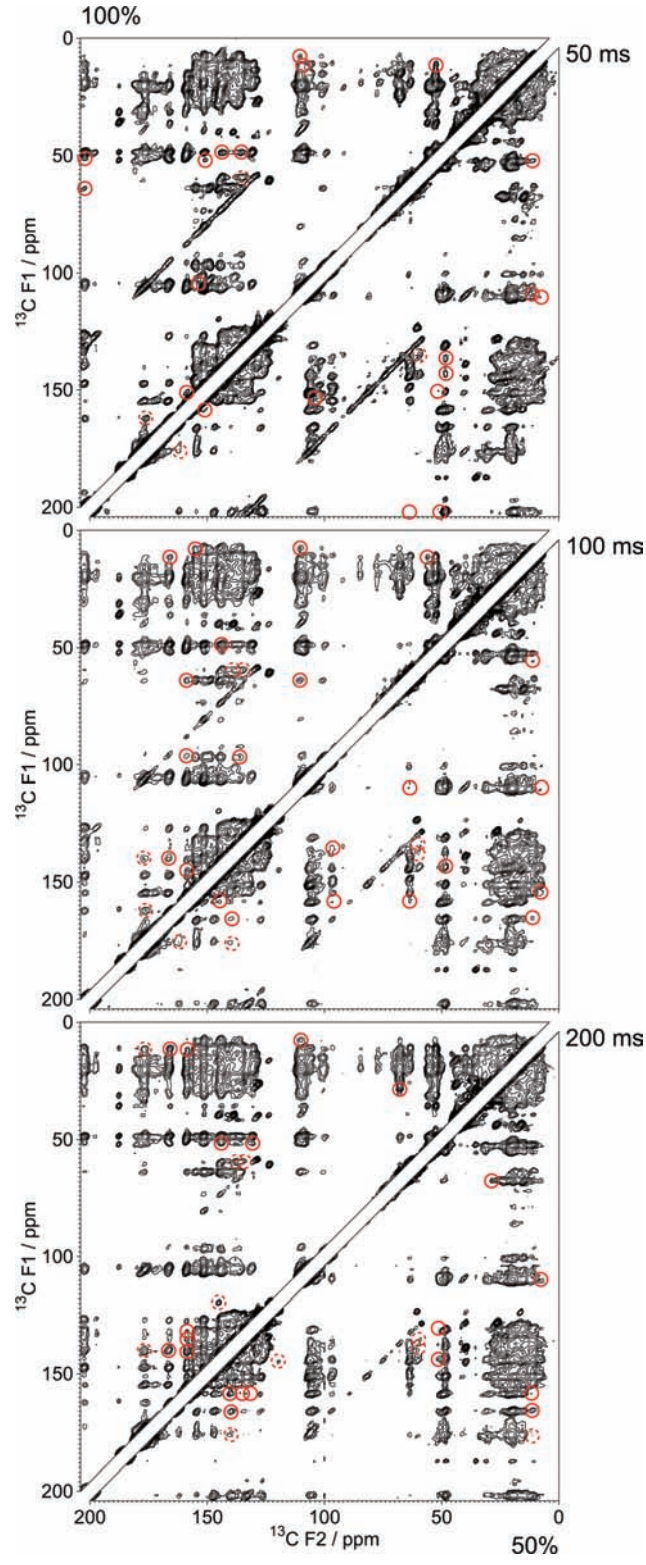

FIGURE 2: DARR spectra of reassembled chlorosome containing 100% [^{13}C]BChl *c* (each top-left triangle) and 50% [^{13}C]BChl *c* (each bottom-right triangle) recorded with mixing times of 50, 100, and 200 ms (each spectrum was symmetrized). The *intermolecular* $^{13}C\cdots^{13}C$ magnetic-dipole correlation peaks, whose intensities decreased into $\sim^{1}/_{4}$ on going from 100% to 50% [^{13}C]BChl *c*, are shown in red solid and red broken circles for the macrocycle and the farnesyl side chain, respectively. The correlation peaks thus identified are listed in Table 1.

Table 1: Intermolecular $^{13}C\cdots{}^{13}C$ Dipolar Correlation Peaks Identified in the DARR Spectra Recorded at Different Mixing Times

50 ms	100 ms	200 ms
1/6	$1/3^1$	1/7
(3 or 12)/13^2	1/4	$1/7^1$
$3^1/13^1$	1/5	1/8
6/(15 or 20)	(3 or 12)/13^2	2/16
$7/13^2$	(3 or 12)/14	(3 or 12)/14
$7^1/10$	(3 or 12)/17^3	(3 or 12)/(17 or 18)
$7^1/13^2$	$3^1/10$	$3^1/8^1$
7^1/(15 or 20)	5/7	$7^1/10$
(9 or 11)/(17 or 18)	$6/7^1$	$7^1/14$
13^1/(17 or 18)	$7^1/10$	$7^1/17^3$
$14/17^3$	$7^1/14$	$8/17^3$
F1/F11	7^1/(17 or 18)	13/(17 or 18)
	$14/17^3$	F1/F7
	F1/F7	F1/F11
	F1/F11	F2/F3

gives rise to very severe collisions between the pair of side chains (not shown); therefore, the construction of this stacking was *not practical* at all. (d) Strongly overlapped dimers forming inclined columns nicely predict most of the observed correlation peaks, except for those in the central part of this particular presentation. The averaged score of agreement is as high as 68%.

(e) Weakly overlapped dimers forming aligned layers do not explain the observed correlation peaks so well; many peaks in the diagonal and off-diagonal regions are left unexplained. The averaged score of agreement is as low as 51%. (f) Weakly overlapped dimers forming displaced layers, whose stacking motif was first found in solid aggregate (*19*), explain best the observed correlation peaks and exhibit the highest averaged score of agreement, i.e., 84%. Table 2 shows that the score of agreement at the mixing time of 200 ms for this particular stacking (f), i.e., 90%, is much higher than those for other stackings (a)−(e), i.e., 40−70%.

In conclusion, the stacking of (f) "weakly overlapped dimers forming displaced layers" is selected as the most plausible stacking, which explains best the observed intermolecular $^{13}C\cdots{}^{13}C$ magnetic-dipole correlations.

Difference in Stacked Structures in Chlorosome and in Solid Aggregate Probed by X-Ray Diffraction. (A) Crucial Role of Water for the Integrity of the Chlorosome Structure.

Figure 4 compares the X-ray diffraction patterns for intact and reassembled chlorosomes (the top two), solid aggregate (the bottom), and during the processes of dehydration in chlorosome (in between). The X-ray diffraction of chlorosome was measured, while keeping the humidity, by placing a wet sample mounted on a ground glass and a tiny water bottle in a housing equipped with a Teflon lid and window (*20*). The X-ray diffraction pattern of chlorosome is well structured and gives rise to a set of multiple diffraction peaks, whereas that of solid aggregate exhibits only a pair of major broad profiles. In particular, the lowest angle diffraction peak at 23.8 Å uniquely appears in chlorosome.

When chlorosome was partially dehydrated, the diffraction peak at 3.5 Å decreases in intensity relative to that at 4.5 Å, and the diffraction peak at 23.8 Å shifts to 22.8 Å. When chlorosome was freeze-dried, the 3.5 Å diffraction peak disappeared completely, the 23.8 Å peak shifted even down to 21.6 Å, and the 2.2 Å peak shifted to 2.1 Å, decreasing its intensity. When the sample was completely dehydrated by evacuating by a pump, the diffraction pattern became indistinguishable from that of solid aggregate. The above series of changes in the X-ray diffraction pattern indicate that the stacking structure in chlorosome can transform into that in the solid aggregate by the complete removal of water. Therefore, the peaks at 23.8, 3.5, and 2.2 Å in intact chlorosome can be correlated with the binding of water molecule(s) to the same stacking of macrocycles as in solid aggregate. At an early stage of dehydration, a reverse change was observed by addition of water; however, we are still unable to transform the stacking structure in solid aggregate into that in chlorosome by incubating with water.

Most importantly, we have found that the presence of water is crucial for the integrity of the stacked structure in chlorosome.

(B) Dependence of the Calculated X-Ray Diffraction Pattern on the Stacking Structure and Selection of the Most Plausible Stacking of Macrocycles. Figure 5 reproduces the six different types of stacking of macrocycles shown in Figure 1. In each stacking, the size and shape of each asymmetric unit (circled by dotted line) and its arrangement specified by the distances along the *a* and *b* axes are uniquely determined. The X-ray diffraction patterns were calculated based on the set of regular two-dimensional arrangement, the results of which are presented in Figure 6 (the bottom six sets of diffraction lines). The calculated diffraction patterns can be characterized as follows.

(i) The region where the calculated diffraction peaks appear depends on the size of the asymmetric unit: It is the smallest in the monomer-based stacking, (a) and (b), where a single BChl *c* molecule constitutes the asymmetric unit; it is medium in the dimer-based stacking, (d), (e), and (f), where a single piggyback dimer constitutes the asymmetric unit; it is the largest in another dimer-based stacking, (c), where a pair of stacked piggyback dimers constitutes the asymmetric unit.

(ii) When we focus our attention on the skeleton of macrocycle, their arrangements in weakly overlapped monomers, (a) and (b), are the same, and therefore, they give rise to the same diffraction pattern. By the same token, weakly overlapped dimers, (e) and (f), give rise to basically the same diffraction pattern.

(iii) As far as the *regular* two-dimensional arrangement is assumed, the lowest angle diffraction peak at 23.8 Å can never be explained. This diffraction peak is ascribable to a completely different origin.

Figure 6 (the top two) presents the observed diffraction peaks in chlorosome and in solid aggregate. In chlorosome, we observed no clear diffraction peaks around 14 Å at all (see Figure 4). However, the X-ray diffraction is *not zero* in this particular region. We found that the stacking structures probed by the intermolecular $^{13}C\cdots{}^{13}C$ correlations are the same between chlorosome and solid aggregate; actually, the 14.1 Å diffraction is explained by the distance between the stacked columns of the same type of macrocycles (see Figure 7a). Therefore, we can safely assume the presence of such a diffraction peak in this particular region.

Now, we are going to select the most plausible stacking based on comparison between the observed and calculated diffraction patterns (see Figure 6). At the first glance, we notice that the observed diffraction patterns are nicely predicted by the stackings, i.e., weakly overlapped dimers forming either (e) aligned layers or (f) displaced layers.

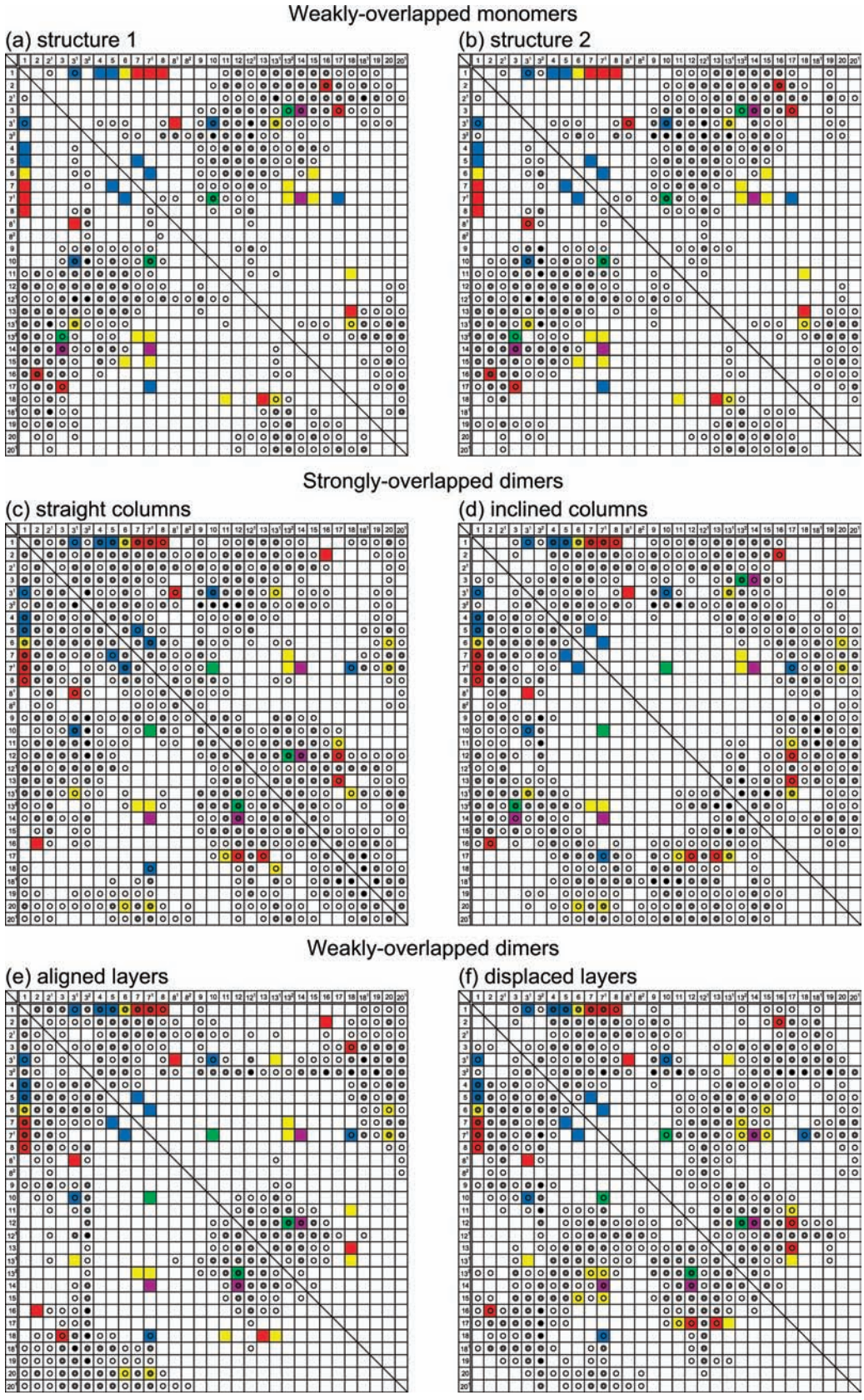

FIGURE 3: Comparison between the observed *intermolecular* $^{13}C\cdots{}^{13}C$ magnetic-dipole correlation peaks and the nearest-neighbor carbon-to-carbon close contacts simulated for the various stackings of macrocycles that are shown in Figure 1. The observed correlation peaks are classified by mixing times in color: 50 ms (yellow), 100 ms (blue), 200 ms (red), 50 and 100 ms (green), and 100 and 200 ms (magenta). The simulated carbon-to-carbon close contacts are classified by interatomic distances (r) in different symbols: $r \leq 4$ Å (filled circle), $4 < r \leq 5$ Å (open double circle), and $5 < r \leq 6$ Å (open single circle). The scores of agreement are listed in Table 2.

Therefore, these stackings can be proposed as the most plausible stackings. (The origins of typical calculated diffraction peaks are depicted in Figure 7a by the use of the stacking (f) as an example.) On the contrary, the monomer-

Table 2: Scores of Agreement (in %) in the Prediction of Intermolecular Correlation Peaks for Different Models[a]

	weakly overlapped monomers		strongly overlapped dimers		weakly overlapped dimers	
ms	(a) structure 1	(b) structure 2	(c) straight columns	(d) inclined columns	(e) aligned layers	(f) displaced layers
50	40	40	70	70	40	80
100	45	45	82	64	64	82
200	40	50	70	70	50	90
average	42	45	74	68	51	84

[a] The scores are defined as the number of the correctly predicted correlation peaks divided by the number of the total correlation peaks observed.

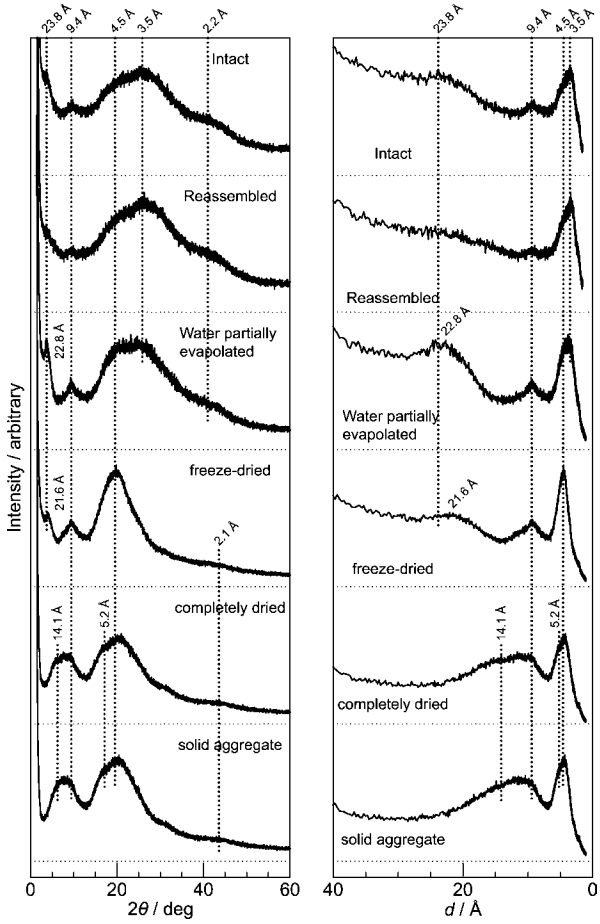

FIGURE 4: X-ray diffraction patterns of intact and reassembled chlorosomes (top two), that of solid aggregate (bottom), and changes in the X-ray diffraction pattern caused by the removal of water from intact chlorosome (middle).

based stacking, (a) structure 1 or (b) structure 2, or (d) strongly overlapped dimers forming inclined columns exhibit no diffraction peaks around 14 Å. (c) Strongly overlapped dimers forming straight columns predict an additional diffraction peak as high as at 18.0 Å contradictory to the observation.

(C) Location of the Binding Sites of Water Molecules in Chlorosome. Searching for the binding pockets of water molecules based on the plausible stacking of macrocycles, i.e., (f) weakly overlapped dimers forming displaced layers (selected by both the intermolecular $^{13}C\cdots{}^{13}C$ magnetic-dipole correlations and the X-ray diffraction pattern), leads us to find two pairs of binding pockets (see Figure 7b), i.e., one around the pair of hydroxyethyl oxygen atoms (shown in orange) and the other around the keto-carbonyl oxygen atoms (magenta). (It is to be noted that each colored circle stands for a pair of water molecules in this figure.) Figure 8 shows the two *possible* pairs of bound water molecules in the atomic-structure presentation. The model building suggests that the water oxygen-to-hydroxyethyl oxygen distance in the former is longer (3.0−3.4 Å) than the water oxygen-to-keto-carbonyl oxygen distance in the latter (2.8−3.0 Å). These oxygen-to-oxygen distances can be correlated with the broad X-ray diffraction peaked at 3.5 Å, which decreases in intensity and then disappears completely during the processes of dehydration (see Figure 4).

Figure 9 presents an extended stacking structure in chlorosome, which we have proposed. The stacking structure in chlorosome has turned out to be the same as that in solid aggregate as far as the intermolecular carbon-to-carbon close contacts that were probed by the intermolecular $^{13}C\cdots{}^{13}C$ magnetic-dipole correlations are concerned. As shown in a previous investigation (*19*), the stacking structure in solid aggregate consists of (i) dimer-based stacking, (ii) pseudo-monomer-based stacking of structure 1 type, and (iii) pseudo-monomer-based stacking of structure 2 type (see Figure 7 of ref *19*). The most important difference is that the stacking structure in chlorosome is stabilized by the hydrogen bonding through the water molecules, which forms a linear array of the piggyback dimer (shown in dotted broken line). The repeating distance between the piggyback dimers is estimated to be 21.0 Å, which can give rise to an X-ray diffraction peak, when some disorder is introduced around the hydrogen-bonding water molecules.

The distance is shorter (by slightly more than 10%) than the X-ray diffraction peak actually observed at 23.8 Å in chlorosome (Figure 6). It is an interesting challenge to reveal the mechanism of how this diffraction peak shifts to 22.8 Å and then to 21.6 Å during the processes of dehydration. Introduction of polar water molecules around the strongly polarizable stacked π-conjugated system may cause such systematic changes in the size of the stacked structure.

There still remains the possibility that the 23.8 Å diffraction peak actually reflects a regular *intersheet* stacking bridged by the use of the farnesyl side chains in between (*9, 10*). Actually, such a stacking has been inferred in a chlorophyll *a*/water aggregate (*28, 29*).

Evidence for Dimer-Based Stacking and Axial Binding of a Water Molecule to One of the Macrocycles in the Piggyback Dimer As Revealed by ^{25}Mg NMR Spectroscopy. Figure 10 shows the ^{25}Mg NMR spectra of chlorosome and solid aggregate. The former consists of two signals (hereafter called "signal 1" and "signal 2"), whereas the latter consists of a single signal ("signal 3"). The spectral width is in the order signal 2 < signal 1 < signal 3. The presence of two signals in chlorosome constitutes strong evidence for the dimer-based stacking, and therefore, we have tried to explain this observation in the following steps.

(i) In the ^{25}Mg nucleus having the nuclear spin $I = {}^5/_2$, the spectral width is mainly determined by the quadrupole coupling

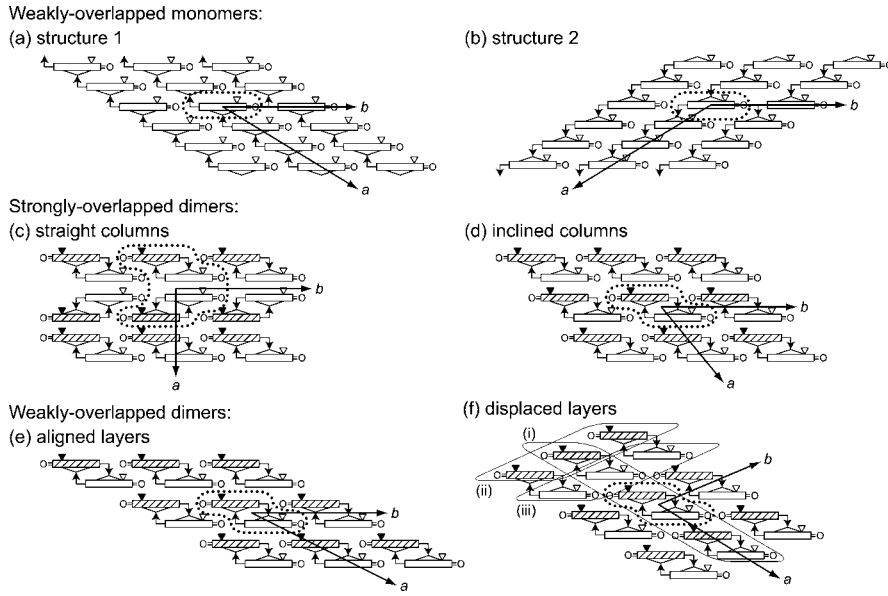

FIGURE 5: Various stackings of macrocycles reproduced from Figure 1. Each stacking exhibits a unique two-dimensional arrangement that is defined by the size and shape of the asymmetric unit (surrounded by dotted line) and by the repeating distance along the *a* and *b* axes in different directions.

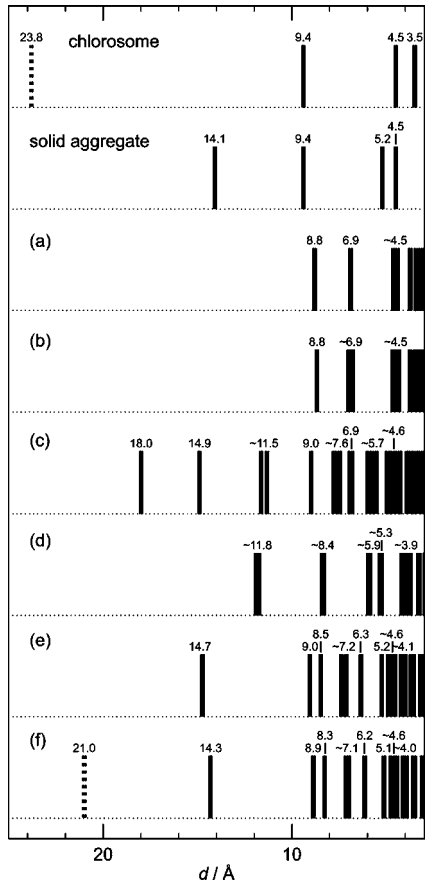

FIGURE 6: Major X-ray diffraction peaks extracted from the diffraction profiles (shown in Figure 4) of intact and reassembled chlorosomes and those simulated for the stackings of macrocycles (a)−(f) (see Figure 5).

constant (e^2qQ), i.e., the quadrupole moment of the nucleus (eQ) multiplied by the electric-field gradient along the symmetry axis (eq). Therefore, the splitting of the ^{25}Mg signal can probe the electric-field gradient on the ^{25}Mg nucleus in the axial direction, when one assumes the same value of the ^{25}Mg quadrupole moment throughout the stacked structure.

(ii) In the BChl *c* macrocycle, the electric-field gradient along the symmetry axis must be strongly influenced by the axial coordination (or interaction). When we compare the pentacoordinated and hexacoordinated states, for example, the electric-field gradient should be very large in the pentacoordinated state due to the asymmetric presence of a single axial ligand and negligible in the hexacoordinated state having the same type of two axial ligands in the same distance from the macrocycle (where the electric-field gradient becomes practically zero). In the particular case of BChl *c* in chlorosome, the pentacoordinated state has been determined by Raman spectroscopy (*30*), and therefore, we have to exclude the possibility of the hexacoordinated state. However, the effect of a sixth ligand *not* expanding the macrocycle to cause the lowering of the ring-breathing frequency that is probed by Raman spectroscopy *but* lowering the electric-field gradient that is probed by the width of the ^{25}Mg NMR signal is still a possibility. Then, the width of the ^{25}Mg NMR must depend on the distance of a sixth ligand in the axial direction. Hereafter, we will call this situation *not* "the hexacoordinated state" *but* "the axial interaction of a sixth ligand".

(iii) In solid aggregate, the macrocycle is definitely in the pentacoordinated state, where the axial ligand is the hydroxyethyl oxygen. Therefore, it is likely that the signal with the largest width, i.e., signal 3, reflects the pentacoordinated state with no additional oxygen in the axial direction, a situation which gives rise to the highest electric-field gradient.

(iv) In chlorosome, on the other hand, the pair of water molecules in the vicinity of the two opposing carbonyl groups (shown in magenta in Figure 8) may play a key role. Signal 1 and signal 2 exhibiting completely different widths strongly suggest that only one of the water molecules is present along the axial direction of the pair of macrocycles facing to each other, either shifted toward *the shadowed macrocycle* in (ii) the pseudo-monomer-based stacking of structure 1 type or shifted toward *the open macrocycle* in (iii) the pseudo-monomer-based stacking of structure 2 type (see Figure 9).

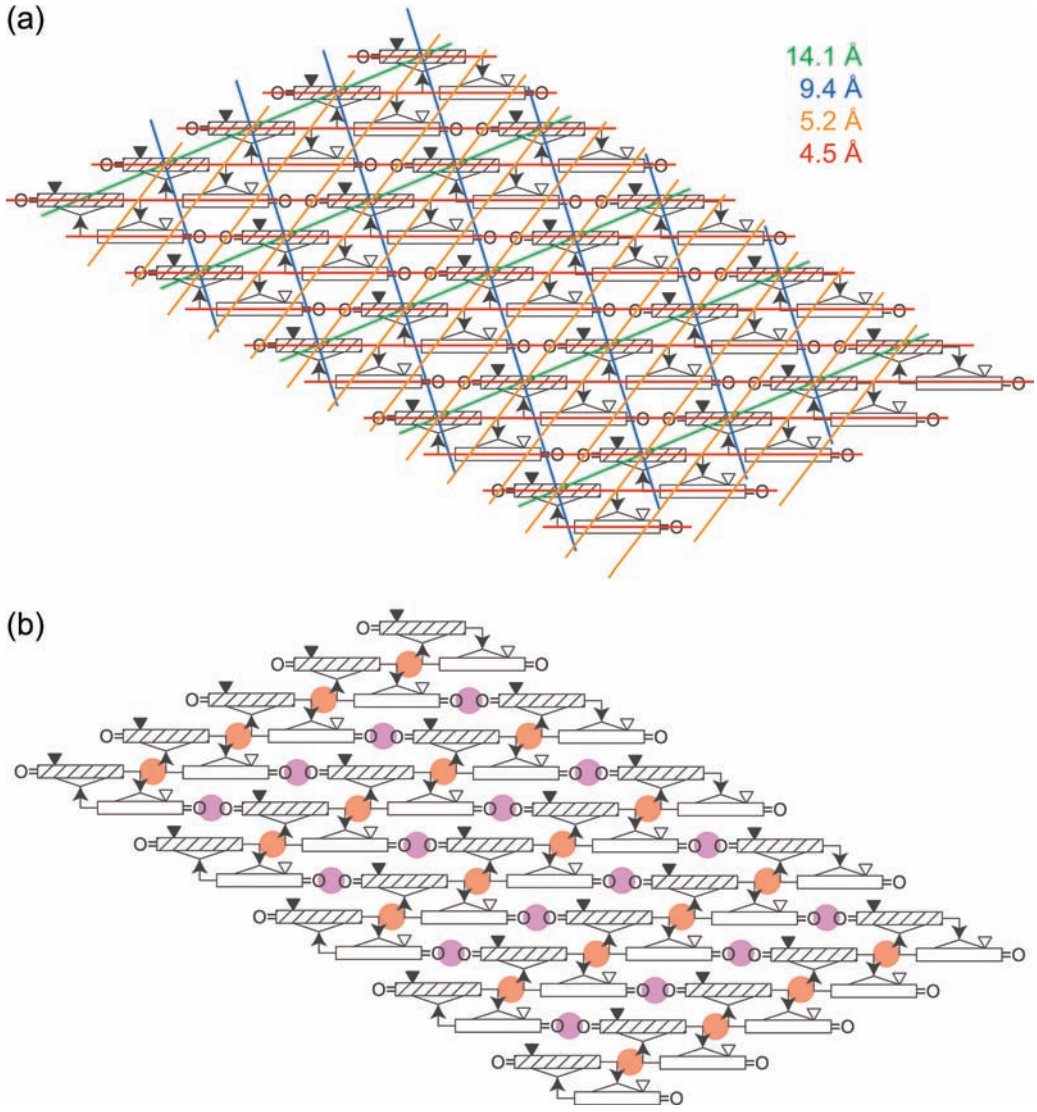

FIGURE 7: (a) Regular arrangements of various components giving rise to major diffraction peaks, originating from the stacking of (f) weakly overlapped dimers forming displaced layers (see Figure 5f for the stacking of macrocycles). (b) Possible pair of binding sites for water molecules in the above-mentioned stacking, i.e., one around the pair of hydroxyethyl oxygen atoms (shown in orange) and the other around the pair of keto-carbonyl oxygen atoms (magenta).

(v) To form the strongest interaction with the water oxygen, the Mg atom binding the hydroxyethyl oxygen as the fifth ligand needs to move toward the macrocycle plane as close as possible. The point is which macrocycle (*shadowed* or *open*) can realize this condition more easily. As seen in Figure 9, in the *shadowed* macrocycle in the monomer-based stacking (ii), the root of the farnesyl side chain (closed triangle) and the hydroxyethyl group (bent arrow) are on the opposite side of the macrocycle, whereas in the *open* macrocycle in the monomer-based stacking (iii), the root of the farnesyl side chain (open triangle) and the hydroxyethyl group (bent arrow) are on the same side of the macrocycle. More precise atomic arrangement is presented in Figure 11. As a result, the large and small green arrows show the large and small magnitude of extrusion of the Mg atom out of the macrocycle plane, respectively, whereas the small blue arrows show the bending part of the farnesyl side chain. Thus, the steric hindrance between the two groups makes the shadowed macrocycle *easier* to achieve the above condition than the open macrocycle.

(vi) In conclusion, the ^{25}Mg nucleus in the shadowed macrocycle must give rise to signal 2 with the narrowest width due to the axial interaction of a water molecule (see Figure 11b), while that in the open macrocycle must give rise to signal 1 with the second widest signal due to practically no axial interaction of the water molecule at all (Figure 11c).

Thus, the pair of the narrow and wide ^{25}Mg signals, reflecting small and large electric-field gradient, has been explained in terms of the presence and absence of a water molecule interacting to the ^{25}Mg nuclei in the axial direction.

Comparison of Our Present Model to Models Proposed by Previous Investigators and Future Trends in the Structural Determination of Chlorosome. Nozawa and co-workers proposed a dimer-based stacking of macrocycles called "a direct ring overlap model" (*13*). The dimer-based stacking itself agrees with our present model, but the dimers do not stack together to form a column in their model (see Figure 8 of ref *13*) contradictory to our model. On the other hand, Holzwarth, de Groot, and co-workers proposed a monomer-based stacking (Figures 5 and 6 of ref *16*) contradictory to our present model of dimer-based stacking, but our model contains two pseudo-monomer-based stackings (ii) and (iii) of structure 1 type and structure 2 type (see Figure 9),

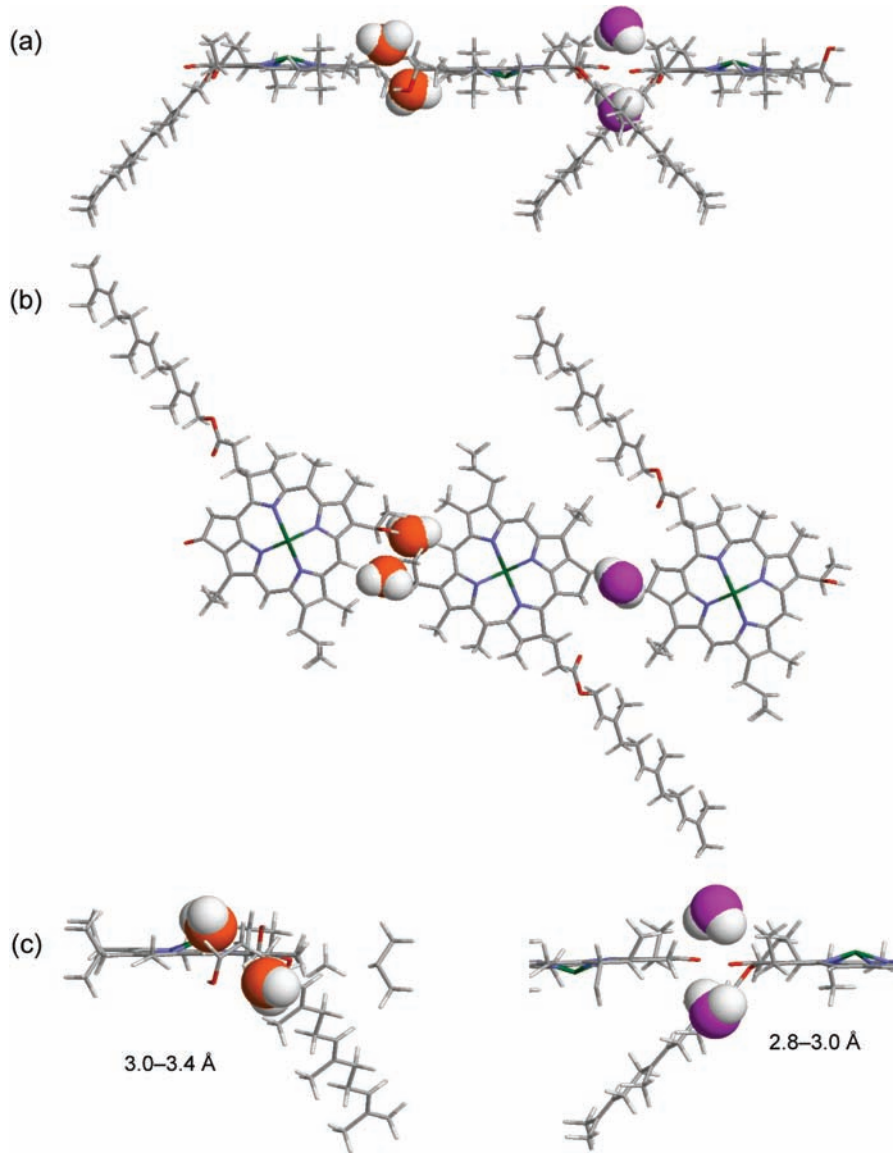

FIGURE 8: Water molecules bound to two possible pairs of binding sites that were identified in the atomic structure of (f) weakly overlapped dimers forming displaced layers. Two different kinds of bound water molecules are shown in different colors as in Figure 7b. Key: (a) side view, (b) top view, and (c) close-up of the binding sites. The figure was drawn by the use of RASMOL (*33*).

respectively. The point is how the ring-current effects can be evaluated, by their calculation, in such a mixture of the dimer-based and pseudo-monomer-based stackings.

Recently, our colleagues challenged to self-consistently determine the assignment of the *intramolecular* and *intermolecular* ^{13}C-dipolar correlation peaks as well as the stacking of macrocycles (in the cylindrical aggregate) by the use of fully ^{13}C-labeled intact chlorosome from *Chl. limicola* we had prepared (*31*). They introduced a polarization-transfer matrix, describing the intensities of the correlation peaks as the functions of the ^{13}C internuclear distance and the mixing time. They started with a set of models with the dimer-based or the monomer-based stackings and eventually reached to a structure of dimer-based stacking (see Figure 4 of ref *31*), which corresponds to our (d) "strongly overlapped dimers forming inclined columns" as far as the short-range stacking of macrocycles is concerned (see Figure 1). Therefore, their model is contradictory to our present model. Most probably, those intramolecular correlation peaks appearing in the diagonal region in the atomic number presentation, which are much stronger than the intermolecular correlation peaks giving rise to the third best score of 68% (see Table 2), should have led the colleagues to a wrong model. The result justifies our rather round about approach to selectively use the *intermolecular* correlation peaks that have been determined *purely spectroscopically* by the use of our reassembled chlorosome.

All of the above three proposed models include the hydrogen bonding between the keto C═O and the hydroxyethyl OH groups, a central dogma originating from the low-frequency shift of the keto C═O stretching vibrational mode. Most recently, however, by a combination of X-ray structural determination and Fourier transform infrared spectroscopy of the model compounds of chlorosomal BChls (called "BChl *c*, *d*, or *e* mimics"), Jochum et al. (*32*) showed that the low-frequency shifts could be explained also in terms of intermolecular interaction between the acetyl C═O group and the central zinc atom. On the basis of the results, they proposed a new stacking model for the structure of chlorosome, including both the hydroxyethyl oxygen pentacoordinating to the central Mg atom (with a distance of 2.0 Å) and the keto-carbonyl interacting with the particular Mg atom

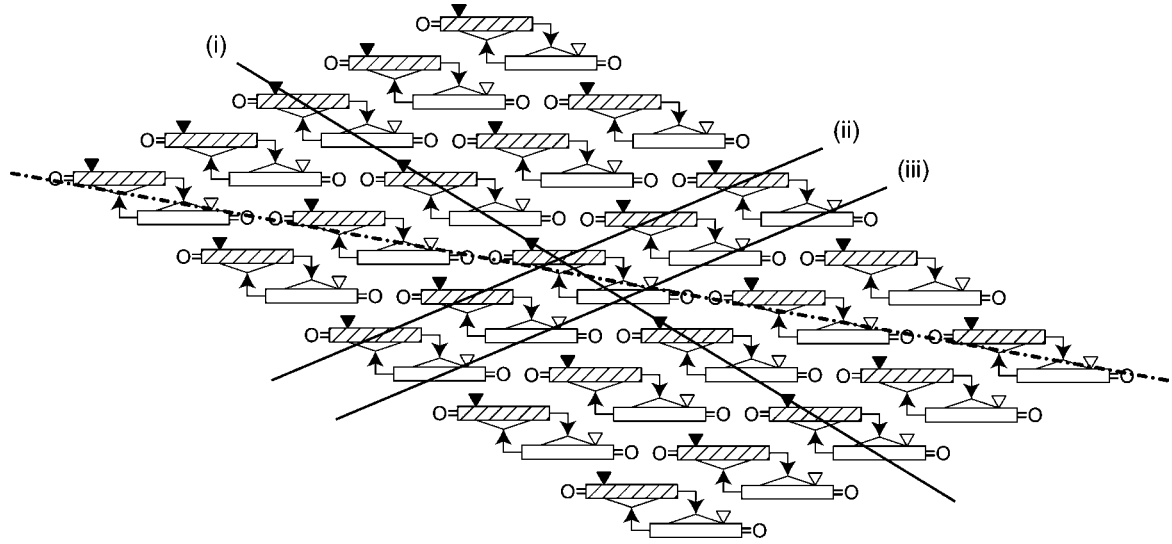

FIGURE 9: An extended sheet for the stacking of macrocycles of (f) weakly overlapped dimers forming displaced layers, which consist of (i) the dimer-based stacking, (ii) the pseudo-monomer-based stacking of structure 1 type, and (iii) the pseudo-monomer-based stacking of structure 2 type. The bound water molecules can form a hydrogen-bonding chain along the dotted-broken line; the spacing between the dimeric asymmetric units is estimated to be 21.0 Å.

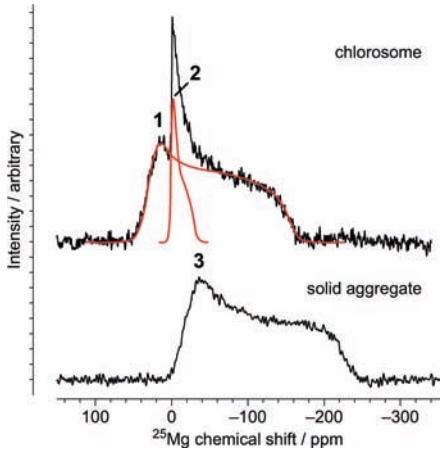

FIGURE 10: ^{25}Mg NMR spectra of intact chlorosome and solid aggregate. Chlorosome exhibits a pair of signals with wide (signal 1) and narrow (signal 2) bandwidths (see the manual decomposition of the profile), whereas solid aggregate exhibits a single signal with the widest bandwidth (signal 3).

(with a distance of 3.3 Å) (the pair of coordination and interaction is called "a $5^1/_2$ coordinated state"; see Figure 6 of ref *32*).

Their proposal is similar to ours in a sense, because at least one of the keto-carbonyl oxygens in the axial position is interacting to the central Mg atom, to which the hydroxyethyl oxygen is coordinating as the fifth ligand (see Figure 1f). The pair of oxygen atoms can be regarded as "the $5^1/_2$-coordinated state" in their terminology.

It is also interesting to compare their X-ray structure of 4-Zn (see Figure 4b of ref *32*) to our model (Figure 1f). When the Zn atom is positioned out of the macrocycle plane, along the perpendicular axis, to form both a coordination with a shorter distance and an axial interaction with a longer distance, between the two acetyl oxygens and the central Zn atom, we can form a column in our (f) "weakly overlapped dimers forming displaced layers". The split C═O stretching IR bands support this interpretation (see Figure 3c of ref *32*).

This type of approach, i.e., a combination of single-crystal X-ray crystallography and some spectroscopic technique(s) that are applied to model compounds, including porphyrin derivatives and modified chlorosomal BChls, can be most powerful in the elucidation of the basic skeleton of chlorosome, even without the water molecules that are modifying and stabilizing the chlorosome structure.

CONCLUSION

The following answers to the questions addressed in the introduction have been obtained in the present investigation:

(1) Does the aggregate structure in chlorosome consist of the monomer-based stacking or the dimer-based stacking? It consists of dimer-based stacking. The stacking named (f) weakly overlapped dimers forming displaced layers has been selected as the most plausible stacking by comparison between the intermolecular $^{13}C\cdots{}^{13}C$ magnetic-dipole correlations and the simulated nearest-neighbor carbon-to-carbon close contacts *as well as* by comparison of the observed X-ray diffraction peaks (profile) with the simulated diffraction peaks, both based on a set of various stackings of macrocycles so far identified. In particular, ^{25}Mg NMR spectroscopy of chlorosome exhibited two different signals with wide and narrow widths as definitive evidence for the dimer-based stacking.

(2) What is the relation in the stacking of macrocycles between chlorosome and solid aggregate? It is *basically* the same. As mentioned above, the stacking of (f) weakly overlapped dimers forming displaced layers has been selected for chlorosome in the present investigation. The same stacking motif was selected for solid aggregate in a previous investigation (*19*). In particular, X-ray diffraction patterns of chlorosome actually transformed into that of solid aggregate after the complete removal of water, a crucial evidence for the direct correlation between the stacked structure in chlorosome and that in solid aggregate.

(3) What is the specific role of water molecules in the aggregate structure in chlorosome? Water molecules are an essential component to keep the integrity of the aggregate

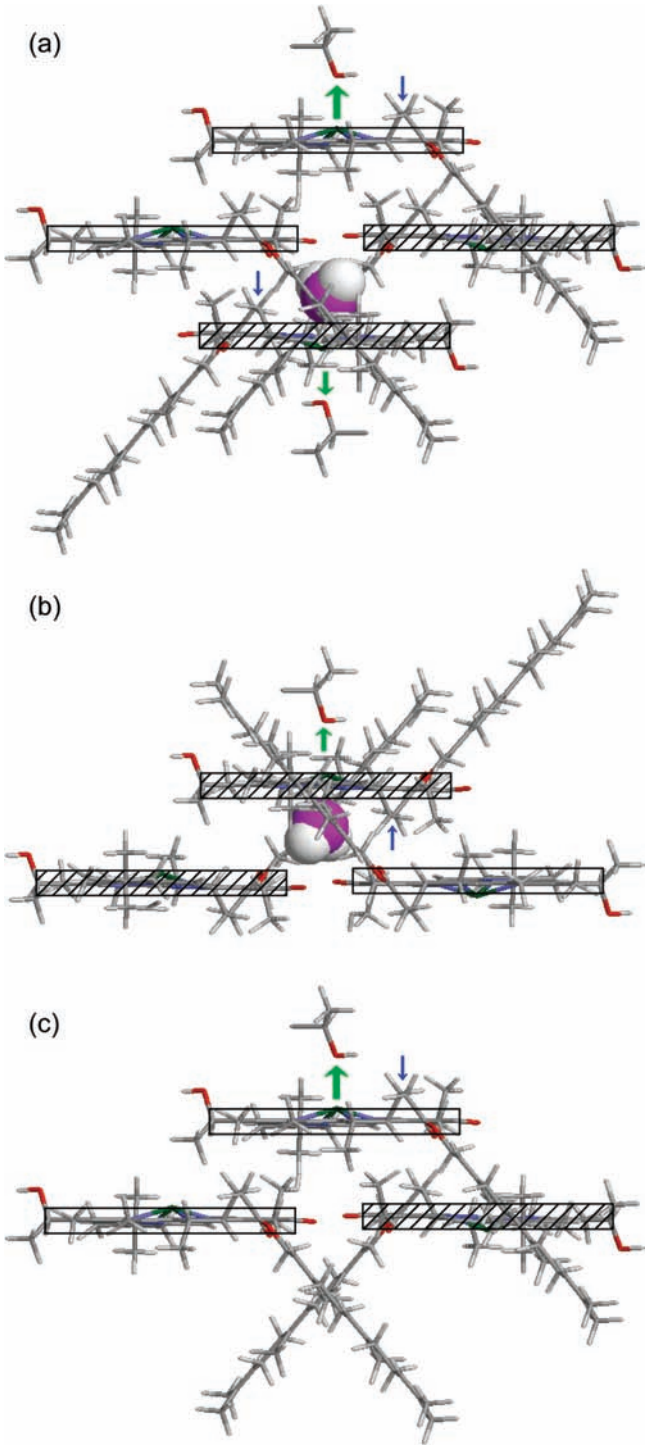

FIGURE 11: (a) Asymmetric occupation, by a single water molecule, at one of the water-binding sites around the keto-carbonyl oxygen atoms (see Figure 8), which explains the ^{25}Mg NMR spectrum of chlorosome exhibiting two signals with wide and narrow bandwidths (see Figure 10). (b) The presence of a water molecule in the axial position of the shadowed macrocycle, forming the pseudo-monomer-based stacking of structure 1 type, and (c) the absence of such a water molecule in the axial position of the open macrocycle, forming the pseudo-monomer-based stacking of structure 2 type (see Figure 9). The direction of the partial structure in (a) is reversed in (b) to facilitate comparison with the partial structure in (c) that is reproduced from (a) keeping the orientation. The large and small green arrows indicate the large and small shifts of the central Mg atom out of the macrocycle plane. The small blue arrow indicates the bent position of the farnesyl side chain, which is located on (b) the opposite and (c) the same side of the extruding Mg atom with respect to the macrocycle plane. The figure was drawn with RASMOL (*33*).

structure in chlorosome. Dehydration degraded and eventually destroyed the aggregate structure in chlorosome as probed by X-ray diffraction. Analysis of an atomic model structure, based on the stacking of (f) weakly overlapped dimers forming displaced layers, identified possible two pairs of water binding sites, i.e., one around the hydroxyethyl oxygen atoms and the other around the keto-carbonyl oxygen atoms. The pair of ^{25}Mg NMR signals with different magnitudes of quadrupole interaction showed that only one of the *latter* binding sites was actually occupied by a water molecule. The number of water molecules bound to the former binding sites has not been determined yet. Further investigation is necessary to correlate the shift of the 23.8 Å X-ray diffraction peak to the changes in the aggregate structure in chlorosome during the processes of dehydration.

(4) What is the relevance of the overall aggregate structure in chlorosome to its physiological functions? Two different functions, i.e., one, mechanical stabilization of the stacked structure, and the other, efficient singlet-energy transfer within the sheet of the stacked macrocycles, can be proposed (see Figure 9): The stacking of macrocycles, which has been identified in the present investigation, can extend to form a sheet structure, which is expected to be stabilized by the displaced layers of macrocycles belonging to different piggyback dimers and by the hydrogen bonding through water molecules connecting the dimeric units. On the other hand, the closely stacked π-conjugated macrocycles along (i) the dimer-based stacking, (ii) the pseudo-monomer-based stacking of structure 1 type, and (iii) pseudo-monomer-based stacking of structure 2 type can provide three different energy-transfer pathways of the coherent singlet excitation to any position in the widely extended sheet structure.

The present investigation has shown the essential role of water molecules in stabilizing the aggregate structure in chlorosome and provided some insight into the water binding sites. The results suggest that the cryoelectron microscopy of chlorosome on *vitreous ice* should provide more reliable structural information than the electron microscopy of freeze-fractured chlorosome at room temperature. Finally, we would like to suggest that the sheet structure shown in Figure 9 may constitute a basic structure for the multilayer structures shown in Figures 3 and 4 of ref *10* (see also Figures 1 and 3 of ref *11*).

(One of the reviewers advised us to examine the possibility of a mixed structure consisting of stackings (a), (b), and (f) in Figure 1; our response is presented in Supporting Information.)

ACKNOWLEDGMENT

The authors thank Mr. Hiroshi Yoshioka, Faculty of Science and Technology, Kwansei Gakuin University, for technical assistance in the measurement of X-ray diffraction patterns.

SUPPORTING INFORMATION AVAILABLE

Details of the assignment of the ^{13}C signals, concerning the macrocycle and farnesyl side chain, in the DARR spectrum of reassembled chlorosome containing 100% [^{13}C]BChl *c* (Figure S1) and a note responding to one of the reviewer's comments to examine the possibility of a mixed

structure. This material is available free of charge via the Internet at http://pubs.acs.org.

REFERENCES

1. Blankenship, R. E., and Matsuura, K. (2003) Antenna Complexes from Green Photosynthetic Bacteria, in *Light-Harvesting Antennas in Photosynthesis* (Green, B. R., and Parson, W. W., Eds.) pp 195−217, Kluwer Academic Publishers, Dordrecht, The Netherlands.
2. Olson, J. M. (1998) Chlorophyll organization and function in green photosynthetic bacteria. *Photochem. Photobiol. 67*, 61–75.
3. Blankenship, R. E., Olson, J. M., and Miller, M. (1995) Antenna Complexes from Green Photosynthetic Bacteria, in *Anoxygenic Photosynthetic Bacteria* (Blankenship, R. E., Madigan, M. T., and Bauer, C. E., Eds.) pp 399−435, Kluwer Academic Publishers, Dordrecht, The Netherlands.
4. Oelze, J., and Golecki, J. R. (1995) Membranes and Chlorosomes of Green Bacteria: Structure, Composition and Development, in *Anoxygenic Photosynthetic Bacteria* (Blankenship, R. E., Madigan, M. T., and Bauer, C. E., Eds.) pp 259−278, Kluwer Academic Publishers, Dordrecht, The Netherlands.
5. Cohen-Bazire, G., Pfennig, N., and Kunisawa, R. (1964) The fine structure of green bacteria. *J. Cell Biol. 22*, 207–225.
6. Staehelin, L. A., Golecki, J. R., Fuller, R. C., and Drews, G. (1978) Visualization of the supramolecular architecture of chlorosomes (*Chlorobium* type vesicles) in freeze-fractured cells of *Chloroflexus aurantiacus*. *Arch. Microbiol. 119*, 269–277.
7. Staehelin, L. A., Golecki, J. R., and Drews, G. (1980) Supramolecular organization of chlorosomes (*Chlorobium* vesicles) and of their membrane attachment sites in *Chlorobium limicola*. *Biochim. Biophys. Acta 589*, 30–45.
8. Wullink, W., and van Bruggen, E. F. J. (1988) Structural Studies on Chlorosomes from *Prosthecochloris aestuarii*, in *Green Photosynthetic Bacteria* (Olson, J. M., Ormerod, J. G., Amesz, J., Stackebrandt, E., and Trüper, H. G., Eds.) pp 3−14, Plenum Press, New York.
9. Pšenčík, J., Ikonen, T. P., Laurinmäki, P., Merckel, M. C., Butcher, S. J., Serimaa, R. E., and Tuma, R. (2004) Lamellar organization of pigments in chlorosomes, the light harvesting complexes of green photosynthetic bacteria. *Biophys. J. 87*, 1165–1172.
10. Oostergetel, G. T., Reus, M., Chew, A. G. M., Bryant, D. A., Boekema, E. J., and Holzwarth, A. R. (2007) Long-range organization of bacteriochlorophyll in chlorosomes of *Chlorobium tepidum* investigated by cryo-electron microscopy. *FEBS Lett. 581*, 5435–5439.
11. Linnanto, J. M., and Korppi-Tommola, J. E. I. (2008) Investigation on chlorosomal antenna geometries: tube, lamella and spiral-type self-aggregates. *Photosynth. Res. 96*, 227–245.
12. Nozawa, T., Ohtomo, K., Suzuki, M., Nakagawa, H., Shikama, Y., Konami, H., and Wang, Z.-Y. (1994) Structures of chlorosomes and aggregated BChl *c* in *Chlorobium tepidum* from solid state high resolution CP/MAS ^{13}C NMR. *Photosynth. Res. 41*, 211–223.
13. Nozawa, T., Ohtomo, K., Suzuki, M., Morishita, Y., and Madigan, M. T. (1993) Structures and organization of bacteriochlorophyll *c*'s in chlorosomes from a new thermophilic bacterium *Chlorobium tepidum*. *Bull. Chem. Soc. Jpn. 66*, 231–237.
14. Holzwarth, A. R., and Schaffner, K. (1994) On the structure of bacteriochlorophyll molecular aggregates in the chlorosomes of green bacteria. A molecular modelling study. *Photosynth. Res. 41*, 225–233.
15. Balaban, T. S., Holzwarth, A. R., Schaffner, K., Boender, G.-J., and de Groot, H. J. M. (1995) CP-MAS ^{13}C-NMR dipolar correlation spectroscopy of ^{13}C-enriched chlorosomes and isolated bacteriochlorophyll *c* aggregates of *Chlorobium tepidum*: The self-organization of pigments is the main structural feature of chlorosomes. *Biochemistry 34*, 15259–15266.
16. van Rossum, B.-J., Steensgaard, D. B., Mulder, F. M., Boender, G. J., Schaffner, K., Holzwarth, A. R., and de Groot, H. J. M. (2001) A refined model of the chlorosomal antennae of the green bacterium *Chlorobium tepidum* from proton chemical shift constraints obtained with high-field 2-D and 3-D MAS NMR dipolar correlation spectroscopy. *Biochemistry 40*, 1587–1595.
17. Wang, Z.-Y., Umetsu, M., Kobayashi, M., and Nozawa, T. (1999) ^{13}C- and ^{15}N-NMR studies on the intact bacteriochlorophyll *c* dimers in solutions. *J. Am. Chem. Soc. 121*, 9363–9369.
18. Wang, Z.-Y., Umetsu, M., Kobayashi, M., and Nozawa, T. (1999) Complete assignment of ^{1}H NMR spectra and structural analysis of intact bacteriochlorophyll *c* dimer in solution. *J. Phys. Chem. B 103*, 3742–3753.
19. Kakitani, Y., Nagae, H., Mizoguchi, T., Egawa, A., Akiba, K., Fujiwara, T., Akutsu, H., and Koyama, Y. (2006) Assembly of a mixture of isomeric BChl *c* from *Chlorobium limicola* as determined by intermolecular ^{13}C−^{13}C dipolar correlations: Coexistence of dimer-based and pseudo-monomer-based stackings. *Biochemistry 45*, 7574–7585.
20. Kakitani, Y., Harada, K.-i., Mizoguchi, T., and Koyama, Y. (2007) Isotopic replacement of pigments and a lipid in chlorosomes from *Chlorobium limicola*: Characterization of the resultant chlorosomes. *Biochemistry 46*, 6513–6524.
21. Wahlund, T. M., Woese, C. R., Castenholz, R. W., and Madigan, M. T. (1991) A thermophilic green sulfur bacterium from New Zealand hot springs, *Chlorobium tepidum* sp. nov. *Arch. Microbiol. 156*, 81–90.
22. Takegoshi, K., Nakamura, S., and Terao, T. (2003) ^{13}C−^{1}H dipolar-driven ^{13}C−^{13}C recoupling without ^{13}C rf irradiation in nuclear magnetic resonance of rotating solids. *J. Chem. Phys. 118*, 2325–2341.
23. Mizoguchi, T., Matsuura, K., Shimada, K., and Koyama, Y. (1996) The structure of the aggregate form of bacteriochlorophyll *c* showing the Q_y absorption above 740 nm: A ^{1}H-NMR study. *Chem. Phys. Lett. 260*, 153–158.
24. Mizoguchi, T., Sakamoto, S., Koyama, Y., Ogura, K., and Inagaki, F. (1998) The structure of the aggregate form of bacteriochlorophyll *c* showing the Q_y absorption above 740 nm as determined by the ring-current effects on ^{1}H and ^{13}C nuclei and by the ^{1}H−^{1}H intermolecular NOE correlations. *Photochem. Photobiol. 67*, 239–248.
25. Mizoguchi, T., Ogura, K., Inagaki, F., and Koyama, Y. (1999) The structure of an aggregate form of bacteriochlorophyll *c* showing the Q_y absorption at 705 nm as determined by the ring-current effects on ^{1}H and ^{13}C nuclei and by ^{1}H−^{1}H intermolecular NOE correlations. *Biospectroscopy 5*, 63–77.
26. Mizoguchi, T., Limantara, L., Matsuura, K., Shimada, K., and Koyama, Y. (1996) Aggregation forms of 8-ethyl-12-ethyl farnesyl bacteriochlorophyll *c* in methanol-chloroform mixture as revealed by ^{1}H NMR spectroscopy. *J. Mol. Struct. 379*, 249–265.
27. Mizoguchi, T., Hara, K., Nagae, H., and Koyama, Y. (2000) Structural transformation among the aggregate forms of bacteriochlorophyll *c* as determined by electronic-absorption and NMR spectroscopies: Dependence on the stereoisomeric configuration and on the bulkiness of the 8-C side chain. *Photochem. Photobiol. 71*, 596–609.
28. van Rossum, B. J., Schulten, E. A. M., Raap, J., Oschkinat, H., and de Groot, H. J. M. (2002) A 3-D structural model of solid self-assembled chlorophyll *a*/H_2O from multispin labeling and MAS NMR 2-D dipolar correlation spectroscopy in high magnetic field. *J. Magn. Reson. 155*, 1–14.
29. de Boer, I., Bosman, L., Raap, J., Oschkinat, H., and de Groot, H. J. M. (2002) 2D ^{13}C−^{13}C MAS NMR correlation spectroscopy with mixing by true ^{1}H spin diffusion reveals long-range intermolecular distance restraints in ultra high magnetic field. *J. Magn. Reson. 157*, 286–291.
30. Hildebrandt, P., Tamiaki, H., Holzwarth, A. R., and Schaffner, K. (1994) Resonance Raman spectroscopic study of metallochlorin aggregates. Implications for the supramolecular structure in chlorosomal BChl *c* antennae of green bacteria. *J. Phys. Chem. 98*, 2192–2197.
31. Egawa, A., Fujiwara, T., Mizoguchi, T., Kakitani, Y., Koyama, Y., and Akutsu, H. (2007) Structure of the light-harvesting bacteriochlorophyll *c* assembly in chlorosomes from *Chlorobium limicola* determined by solid-state NMR. *Proc. Natl. Acad. Sci. U.S.A. 104*, 790–795.
32. Jochum, T., Reddy, C. M., Eichhöfer, A., Buth, G., Szmytkowski, J., Kalt, H., Moss, D., and Balaban, T. S. (2008) The supramolecular organization of self-assembling chlorosomal bacteriochlorophyll *c*, *d*, or *e* mimics. *Proc. Natl. Acad. Sci. U.S.A. 105*, 12736–12741.
33. Sayle, R. A., and Milner-White, E. J. (1995) RASMOL: Biomolecular graphics for all. *Trends Biochem. Sci. 20*, 374–376.

BI801651W